# Evaluation of Both Linear and Non-Linear Control Strategies for a Shipboard Marine Gantry Crane

Iain A. Martin
*Mechanical and Aerospace Engineering Department*
*Carleton University*
Ottawa, Canada
Iain.Martin@carleton.ca

Rishad A. Irani
*Mechanical and Aerospace Engineering Department*
*Carleton University*
Ottawa, Canada
Rishad.Irani@carleton.ca

***Abstract*—Anti-sway control for shipboard marine cranes is an ongoing control problem. In this paper, a simulation tool was developed to evaluate anti-sway controllers for a five degree-of-freedom shipboard gantry crane, actuated as if at sea. The simulator was developed in MATLAB Simulink and ran in real-time with controllers operating on a National Instruments myRIO. A proportional-integral-derivative controller (PID), a model predictive controller (MPC), a sliding mode controller (SMC) and a fuzzy logic controller (FLC) were developed to track a desired trajectory and dampen out payload sway. The controllers were tested both individually and with input commands shaped by a zero-vibration (ZV), zero-vibration-derivative (ZVD) and zero-vibration-derivative-derivative (ZVDD) input shaper.**

**The PID, SMC and FLC controllers were all capable of both tracking the desired trajectory and dampening payload sway without disturbances from ship motion, with the more complex FLC and SMC showing little improvement over the simpler PID. The MPC was unable to track the desired trajectory without jumping the actuator deadbands. The addition of input shapers provided a greater reduction in payload sway at the cost of a delayed response, with the ZVDD showing the greatest reduction in payload sway and the corresponding longest delay. Given the length of the delays however, it is recommended input shaping only be applied to automated or autonomous crane systems.**

**As designed, none of the controllers were able to successfully track the desired trajectory in the presence of ship motion. With the simulation tool, future work for this system will involve improving the control response to ship motion disturbances, operator-in-the-loop testing and hardware deployment.**

***Index Terms*—Marine crane, Gantry crane, Anti-sway control, Input shaping, PID control, Model predictive control, Sliding mode control, Fuzzy logic control**

## I. Introduction

Gantry cranes are often employed to transport heavy cargo aboard large ships. As a gantry crane is an under-actuated system, operator commands and disturbances from ship motion will result in payload sway. An effective control system for a shipboard gantry crane should be able to follow the trajectory specified by the operator and dampen payload sway to prevent the payload from potentially causing injury or damage.

Crane control has been widely studied in literature, with a comprehensive review conducted in 2017 by Ramli et al. [1]. Applied specifically to marine cranes, a significant focus of current research is non-linear and adaptive closed-loop control systems. In 2017, Qian et al. [2] proposed an adaptive learning controller for an offshore boom crane, and Ngo et al. [3] demonstrated the effectiveness of a fuzzy-tuned, sliding mode controller for an offshore container crane. In 2018, Tuan et al. [4] used an adaptive neural network sliding mode controller to control a shipboard container crane. In 2019, Qian et al. [5] proposed an adaptive tracking controller for shipboard cranes, and Yang et al. [6] presented a neural network-based adaptive controller. However, there appears to be no consensus as to what the preferred control strategy is for shipboard cranes.

Instead of focusing solely on the development of a single non-linear controller, the present study seeks to evaluate the performance of multiple controllers spanning a range of both linear and non-linear control techniques. Four control methodologies were selected for the study: A Proportional-Integral-Derivative (PID) controller, a Model Predictive Controller (MPC), a Sliding Mode Controller (SMC) and a Fuzzy Logic Controller (FLC). All of the controllers will be tested on an identical five degree-of-freedom (dof) gantry crane system, developed as a simulator to allow real-time control by an operator for future operator-in-the-loop testing. The base of the crane will be actuated as if at sea to observe the ability of each control system to track the desired trajectory and dampen payload sway in the presence of ship motion. The simulator will be built in MATLAB Simulink using Simscape Multibody and Simscape Desktop Real-Time, and the controllers developed in LabVIEW Real-Time and deployed to a National Instruments (NI) myRio.

The addition of input shaping for each control system will also be explored. In a review conducted by Conker et al. [7], input shapers prove effective at eliminating vibration in flexible systems. Applying input shaping to a marine crane, each of the four feedback controllers will be combined with a zero-vibration (ZV), zero-vibration-derivative (ZVD) and a zero-vibration-derivative-derivative (ZVDD) input shaper.

The present study seeks to provide an understanding of how different control methodologies compare performing anti-sway control for a shipboard marine gantry crane operating in a real-time, simulated environment. The use of four distinct feedback control systems combined with open-loop input shaping provides insight into the strengths and weaknesses of different control techniques, and a basis for the future development of other controller variants.

Section II of this paper provides an overview of the test



978-0-578-57618-3 ©2019 MTS

system, including a complete mathematical model of the 5-dof gantry crane system, the Simscape Multibody model, and the operation of each controller and input shaper. The controllers are tuned without the addition of ship motion, then tested with both input shaping and ship motion. Section III provides the results of the tuning cases and ship motion study. The paper concludes in section IV with a summary of the findings.

## II. System Overview

Fig. 1 presents a high-level schematic of the simulator. The system allows an operator to control the simulated gantry crane in real-time with immediate visual feedback, and dampen any resulting payload sway. Operator inputs are provided by a USB joystick; joystick inputs are used to provide trajectories for the cart, and push button inputs are used to adjust the length of the cable. The inputs are sent to the myRIO and converted to desired states for the system. The trajectory error is calculated using the current states obtained from the Simscape model. The control action is calculated and sent to the Simscape model, where immediate visual feedback is provided to the operator. The use of the Simscape Desktop Real-Time kernel allows the myRIO to operate in real-time with the Simscape model at a frequency of 100 Hz.

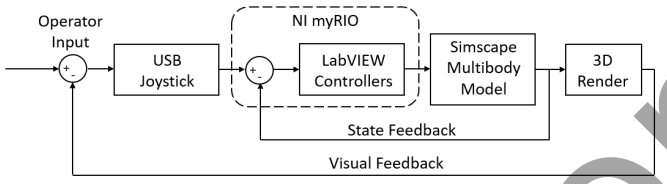


Fig. 1. High-level schematic of the test system.

### A. Mathematical Model of the 5-dof Gantry Crane

To aid in controller development, a mathematical model of the crane system was derived. Fig. 2 presents the free body diagram of the gantry crane. The cart with mass $m_1$ has two translational axes $X$ and $Y$; as the cart moves as a function of time, its positions along the $X$ and $Y$ axes are described by $x(t)$ and $y(t)$, respectively. A payload with mass $m_2$ is free to swing beneath in both the $XZ$ and $YZ$ planes with sway angles $\theta(t)$ and $\phi(t)$, respectively. The cart is actuated by forces $F_x(t)$ and $F_y(t)$ in the $X$ and $Y$ axes, and the cable length $l(t)$ adjusted by a colinear force $F_l(t)$. The mass of the gantry rail is given by $m_{rail}$, and the cable is assumed massless. When ignoring the pendulum mass $m_2$, the effective cart mass in the $y$ axis is $m_{1y} = m_1 + m_{rail}$, while the cart mass in the $x$ axis is simply $m_{1x} = m_1$. Gravity $g$ acts in the negative $Z$ axis of the inertial frame $I$.

The Lagrange approach was used to derive the equations of motion for the gantry crane. As the model has five degrees-of-freedom, five generalized coordinates are needed. The coordinates were taken as the cart positions $x(t)$ and $y(t)$, the cable length $l(t)$, and the sway angles $\theta(t)$ and $\phi(t)$. The position

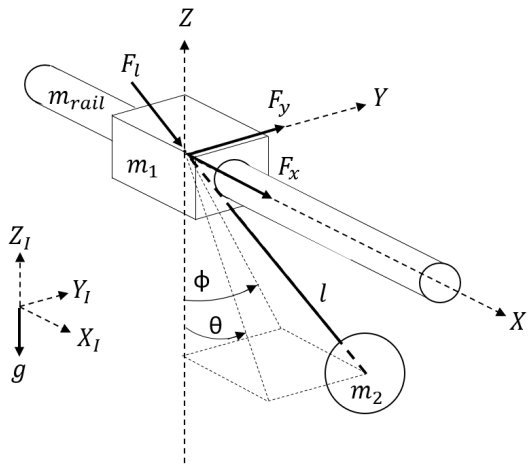


Fig. 2. Free body diagram of the gantry crane.

vectors for the cart $\vec{p}_{cart}$ and payload $\vec{p}_{payload}$ were defined as

$$\vec{p}_{cart} = x(t)\hat{\imath} + y(t)\hat{\jmath} + 0\hat{k}, \tag{1}$$

$$\vec{p}_{payload} = [x(t) + l(t)\sin(\theta(t))]\hat{\imath} + [y(t) + l(t)\sin(\phi(t))]\hat{\jmath} - l(t)\cos(\theta(t))\cos(\phi(t))\hat{k}. \tag{2}$$

The Lagrange equation takes the form

$$\frac{d}{dt}\left(\frac{dT}{d\dot{q}}\right) - \frac{dT}{dq} + \frac{dV}{dq} = F_q \tag{3}$$

where $T$ and $V$ are the total kinetic and potential energies of the system, respectively, $q$ is each generalized coordinate for the system, and $F_q$ is the generalized force corresponding to coordinate $q$. The total kinetic energy of the system $T$ is the summation of the kinetic energies of the cart and payload, such that

$$T = \underbrace{\frac{m_{1x}}{2}\dot{x}(t)^2 + \frac{m_{1y}}{2}\dot{y}(t)^2}_{T_{cart}} + \underbrace{\frac{m_2}{2}\left(\frac{d\vec{p}_{payload}(t)}{dt}\right)^2}_{T_{payload}}. \tag{4}$$

As the cart cannot translate in the $Z$ axis, the only source of potential energy will be due to gravity acting on the payload. The total potential energy $V$ can then be described as

$$V = m_2 g l(t)\cos(\theta(t))\cos(\phi(t)). \tag{5}$$

Evaluating (3), and for notational simplicity dropping $(t)$ from all time-varying quantities, the equations of motion can be expressed in standard form

$$\begin{bmatrix} M_{11} & M_{12} & M_{13} & M_{14} & M_{15} \\ M_{21} & M_{22} & M_{23} & M_{24} & M_{25} \\ M_{31} & M_{32} & M_{33} & M_{34} & M_{35} \\ M_{41} & M_{42} & M_{43} & M_{44} & M_{45} \\ M_{51} & M_{52} & M_{53} & M_{54} & M_{55} \end{bmatrix} \begin{Bmatrix} \ddot{x} \\ \ddot{y} \\ \ddot{l} \\ \ddot{\theta} \\ \ddot{\phi} \end{Bmatrix} + \begin{Bmatrix} a_1 \\ a_2 \\ a_3 \\ a_4 \\ a_5 \end{Bmatrix} = \begin{Bmatrix} F_x \\ F_y \\ F_l \\ 0 \\ 0 \end{Bmatrix} \tag{6}$$

where

$$M_{11} = m_{1x} + m_2 \tag{7}$$
$$M_{22} = m_{1y} + m_2 \tag{8}$$
$$M_{33} = m_2 \sin^2(\phi) + m_2 \sin^2(\theta) + m_2 \cos^2(\phi)\cos^2(\theta) \tag{9}$$
$$M_{44} = m_2 l^2 \cos^2(\theta) + m_2 l^2 \cos^2(\phi)\sin^2(\theta) \tag{10}$$
$$M_{55} = m_2 l^2 \cos^2(\phi) + m_2 l^2 \cos^2(\theta)\sin^2(\phi) \tag{11}$$
$$M_{13} = M_{31} = m_2 \sin(\theta) \tag{12}$$
$$M_{14} = M_{41} = m_2 l \cos(\theta) \tag{13}$$
$$M_{23} = M_{32} = m_2 \sin(\phi) \tag{14}$$
$$M_{25} = M_{52} = m_2 l \cos(\phi) \tag{15}$$
$$M_{34} = M_{43} = m_2 l \cos(\theta)\sin(\theta) - m_2 l \cos^2(\phi)\cos(\theta)\sin(\theta) \tag{16}$$
$$M_{35} = M_{53} = m_2 l \cos(\phi)\sin(\phi) - m_2 l \cos(\phi)\cos^2(\theta)\sin(\phi) \tag{17}$$
$$M_{45} = M_{54} = m_2 l^2 \cos(\phi)\cos(\theta)\sin(\phi)\sin(\theta) \tag{18}$$
$$M_{12} = M_{21} = M_{15} = M_{51} = M_{24} = M_{42} = 0 \tag{19}$$

and

$$a_1 = 2m_2 \dot{l}\dot{\theta}\cos(\theta) - m_2 l \dot{\theta}^2 \sin(\theta) \tag{20}$$
$$a_2 = 2m_2 \dot{l}\dot{\phi}\cos(\phi) - m_2 l \dot{\phi}^2 \sin(\phi) \tag{21}$$
$$\begin{aligned} a_3 = {} & m_2 \dot{l}\dot{\phi}\sin(2\phi) + m_2 \dot{l}\dot{\theta}\sin(2\theta) - m_2 l \dot{\phi}^2 \sin^2(\phi) \\ & - m_2 l \dot{\theta}^2 \sin^2(\theta) - m_2 g \cos(\phi)\cos(\theta) \\ & - m_2 l \dot{\phi}^2 \cos^2(\phi)\cos^2(\theta) - m_2 l \dot{\theta}^2 \cos^2(\phi)\cos^2(\theta) \\ & - 2m_2 \dot{l}\dot{\phi}\cos(\phi)\cos^2(\theta)\sin(\phi) \\ & - 2m_2 \dot{l}\dot{\theta}\cos^2(\phi)\cos(\theta)\sin(\theta) \\ & + 2m_2 l \dot{\phi}\dot{\theta}\cos(\phi)\cos(\theta)\sin(\phi)\sin(\theta) \end{aligned} \tag{22}$$
$$\begin{aligned} a_4 = {} & 2m_2 l \dot{l}\dot{\theta}\cos^2(\theta) + m_2 g l \cos(\phi)\sin(\theta) \\ & - m_2 l^2 \dot{\theta}^2 \cos(\theta)\sin(\theta) + m_2 l^2 \dot{\phi}^2 \cos^2(\phi)\cos(\theta)\sin(\theta) \\ & + m_2 l^2 \dot{\theta}^2 \cos^2(\phi)\cos(\theta)\sin(\theta) \\ & + 2m_2 l \dot{l}\dot{\theta}\cos^2(\phi)\sin^2(\theta) \\ & - 2m_2 l^2 \dot{\phi}\dot{\theta}\cos(\phi)\sin(\phi)\sin^2(\theta) \\ & + 2m_2 l \dot{l}\dot{\phi}\cos(\phi)\cos(\theta)\sin(\phi)\sin(\theta) \end{aligned} \tag{23}$$
$$\begin{aligned} a_5 = {} & 2m_2 l \dot{l}\dot{\phi}\cos^2(\phi) + m_2 g l \cos(\theta)\sin(\phi) \\ & - m_2 l^2 \dot{\phi}^2 \cos(\phi)\sin(\phi) + m_2 l^2 \dot{\phi}^2 \cos(\phi)\cos^2(\theta)\sin(\phi) \\ & + m_2 l^2 \dot{\theta}^2 \cos(\phi)\cos^2(\theta)\sin(\phi) \\ & + 2m_2 l \dot{l}\dot{\phi}\cos^2(\theta)\sin^2(\phi) \\ & - 2m_2 l^2 \dot{\phi}\dot{\theta}\cos(\theta)\sin^2(\phi)\sin(\theta) \\ & + 2m_2 l \dot{l}\dot{\theta}\cos(\phi)\cos(\theta)\sin(\phi)\sin(\theta) \end{aligned} \tag{24}$$

The equations of motion will be used to derive a linearized state-space model for the MPC and to derive the control laws for the SMC. To provide visual feedback for the simulator, Simscape Multibody was used to implement the gantry crane model.

### B. Simscape Multibody Model

Fig. 3 shows the 3D rendering of the Simscape model. The visual model represents a cross section of a ship with a beam of 20 metres. Approximate masses for the crane components were chosen and are presented in Table I. The payload is a small Zodiac-style watercraft, with a mass of 1770 kilograms [8], and the initial cable length $l_0$ is 4 metres.

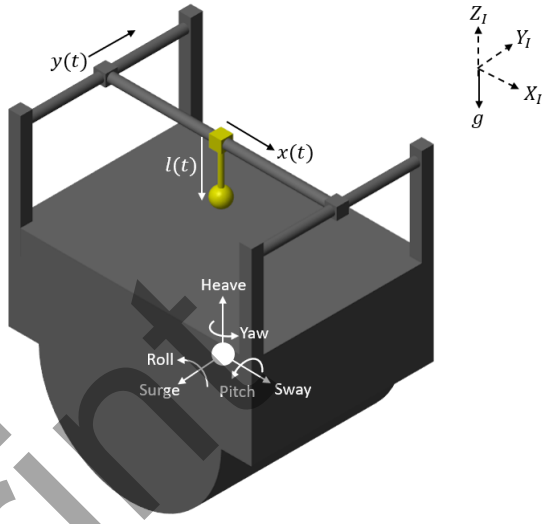


Fig. 3. 3D render of the Simscape model.

TABLE I
CRANE MODEL PARAMETERS

| Parameter | Value |
|---|---|
| $m_1$ | 5000 kg |
| $m_{rail}$ | 10000 kg |
| $m_2$ | 1770 kg |
| $l_0$ | 4.00 m |

Using the parameters presented in Table I, the equations of motion presented in equations (6)-(24) were simulated and validated the results of the Simscape model. Deadbands of $\pm 100$ N and saturation limits of $\pm 50$ kN were added to all of the external forces to observe their effect on the controller performance.

### C. LabVIEW Controllers

Instead of developing the controllers in Simscape along with the Multibody model, the controllers were built in LabVIEW Real-Time and deployed to an NI myRIO to emulate hardware-in-the-loop control. Having the controllers developed in LabVIEW and operating on a myRIO also provides modularity to the system, allowing the Simscape simulator to be replaced with a physical simulator for future studies without redeveloping the controllers.

Four controllers were built for the system: a proportional-integral-derivative (PID) controller, a model predictive controller (MPC), a sliding mode controller (SMC) and a

fuzzy logic controller (FLC). Zero-vibration (ZV), zero-vibration-derivative (ZVD) and zero-vibration-derivative-derivative (ZVDD) input shapers were also developed to test their utility at sway reduction.

*1) Proportional-Integral-Derivative Controller:* Fig. 4 presents the general block diagram of the PID controller implemented in LabVIEW. To evaluate the control actions $u_q$ for each generalized coordinate $q$, where $q = \{x \quad y \quad l \quad \theta \quad \phi\}$, five PID controllers were built that each attempt to minimize the error $e_q$

$$e_q = q_d - q, \tag{25}$$

where $q_d$ is the desired state for coordinate $q$. The proportional, integral and derivative gains corresponding to coordinate $q$ are $K_{P,q}$, $K_{I,q}$ and $K_{D,q}$, respectively, and $T_s$ is the sampling time.

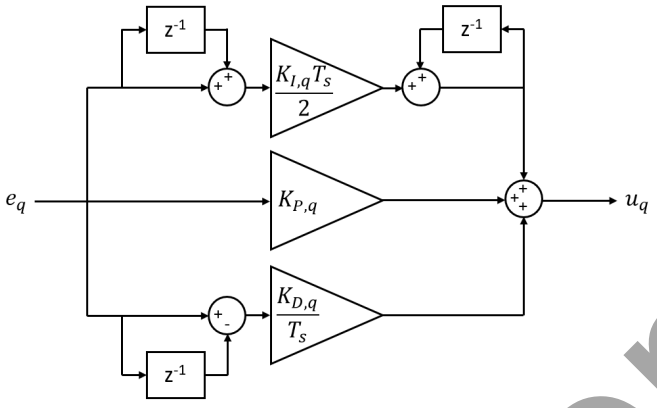


Fig. 4. Block diagram of the discrete-time LabVIEW PID controller.

To implement anti-sway control, the crane must both attempt to track the desired cart trajectory while also drive the pendulum sway angles to zero. To minimize both errors with PID control, $F_x$ and $F_y$ were taken as averages of the control actions calculated by the corresponding PID controllers. Note that if the sway angles are measured as shown in Figure 2, the control actions $u_\theta$ and $u_\phi$ should be negated. The control actions could also be summed instead of averaged, requiring an update to the PID gains. The final forces applied to the Simscape model were

$$F_x = \frac{u_x - u_\theta}{2}, \tag{26}$$

$$F_y = \frac{u_y - u_\phi}{2}, \tag{27}$$

$$F_l = u_l. \tag{28}$$

As the gantry crane system is highly non-linear, traditional linear PID tuning methods such as Root-Locus cannot be directly applied. For the present study, the gains were heuristically tuned as per section III-A.

*2) Model Predicitive Controller:* The MPC uses a linearized model of the system to compute optimal control actions for future timesteps. To obtain a linearized state-space model of the system, the state vector $\mathbf{x}$ and force vector $\mathbf{u}$ were defined as

$$\mathbf{x} = \begin{bmatrix} x & \dot{x} & y & \dot{y} & l & \dot{l} & \theta & \dot{\theta} & \phi & \dot{\phi} \end{bmatrix}^T, \tag{29}$$

$$\mathbf{u} = \begin{bmatrix} F_x & F_y & F_l \end{bmatrix}^T, \tag{30}$$

with the equilibrium conditions

$$\mathbf{x_0} = \begin{bmatrix} 0 & 0 & 0 & 0 & 4 & 0 & 0 & 0 & 0 & 0 \end{bmatrix}^T, \tag{31}$$

$$\mathbf{u_0} = \begin{bmatrix} 0 & 0 & -m_2 g \end{bmatrix}^T. \tag{32}$$

Decoupling the equations of motion presented in section II-A and evaluating the Jacobian at the equilibrium position, the linearized state-space model takes the form

$$\dot{\mathbf{x}} = A\mathbf{x} + B\mathbf{u}, \tag{33}$$

$$\dot{\mathbf{y}} = C\mathbf{x} + D\mathbf{u}, \tag{34}$$

where

$$A = \begin{bmatrix} 0 & 1 & 0 & 0 & 0 & 0 & 0 & 0 & 0 & 0 \\ 0 & 0 & 0 & 0 & 0 & 0 & \frac{m_2 g}{m_{1x}} & 0 & 0 & 0 \\ 0 & 0 & 0 & 1 & 0 & 0 & 0 & 0 & 0 & 0 \\ 0 & 0 & 0 & 0 & 0 & 0 & 0 & 0 & \frac{m_2 g}{m_{1y}} & 0 \\ 0 & 0 & 0 & 0 & 0 & 1 & 0 & 0 & 0 & 0 \\ 0 & 0 & 0 & 0 & 0 & 0 & 0 & 0 & 0 & 0 \\ 0 & 0 & 0 & 0 & 0 & 0 & 0 & 1 & 0 & 0 \\ 0 & 0 & 0 & 0 & 0 & 0 & \frac{-g(m_{1x}+m_2)}{4m_{1x}} & 0 & 0 & 0 \\ 0 & 0 & 0 & 0 & 0 & 0 & 0 & 0 & 0 & 1 \\ 0 & 0 & 0 & 0 & 0 & 0 & 0 & 0 & \frac{-g(m_{1y}+m_2)}{4m_{1y}} & 0 \end{bmatrix}, \tag{35}$$

$$B = \begin{bmatrix} 0 & \frac{1}{m_{1x}} & 0 & 0 & 0 & 0 & 0 & -\frac{1}{4m_{1x}} & 0 & 0 \\ 0 & 0 & 0 & \frac{1}{m_{1y}} & 0 & 0 & 0 & 0 & 0 & -\frac{1}{4m_{1y}} \\ 0 & 0 & 0 & 0 & 0 & \frac{1}{m_2} & 0 & 0 & 0 & 0 \end{bmatrix}^T, \tag{36}$$

$$C = \begin{bmatrix} 1 & 0 & 0 & 0 & 0 & 0 & 0 & 0 & 0 & 0 \\ 0 & 0 & 1 & 0 & 0 & 0 & 0 & 0 & 0 & 0 \\ 0 & 0 & 0 & 0 & 1 & 0 & 0 & 0 & 0 & 0 \\ 0 & 0 & 0 & 0 & 0 & 0 & 1 & 0 & 0 & 0 \\ 0 & 0 & 0 & 0 & 0 & 0 & 0 & 0 & 1 & 0 \end{bmatrix}, \tag{37}$$

and $D$ a 5x3 zero matrix. The controller was implemented using the MPC tools provided in the LabVIEW Control Design and Simulation Module [9]. As the system operates in real-time, the future trajectory considered in the MPC's prediction horizon is not directly known. Instead, all future values for the trajectory were set to the desired trajectory at the current timestep.

*3) Sliding Mode Control:* As the gantry crane system is non-linear, a non-linear controller such as an SMC may provide improved performance over the PID and MPC. In accordance with Slotine and Li [10], the error vector $\mathbf{e}$ is defined as

$$\mathbf{e} = \begin{Bmatrix} x - x_d \\ y - y_d \\ l - l_d \\ \theta - \theta_d \\ \phi - \phi_d \end{Bmatrix}, \tag{38}$$

where the subscript $d$ denotes the desired state. The sliding surface $\mathbf{s}$ is then defined by

$$\mathbf{s} = \dot{\mathbf{e}} + \lambda \mathbf{e}, \tag{39}$$

where

$$\lambda = \begin{bmatrix} \lambda_1 & 0 & 0 & 0 & 0 \\ 0 & \lambda_2 & 0 & 0 & 0 \\ 0 & 0 & \lambda_3 & 0 & 0 \\ 0 & 0 & 0 & \lambda_4 & 0 \\ 0 & 0 & 0 & 0 & \lambda_5 \end{bmatrix}. \tag{40}$$

Taking a derivative of the sliding surface, one obtains

$$\dot{\mathbf{s}} = \ddot{\mathbf{e}} + \lambda \dot{\mathbf{e}} = \ddot{\mathbf{q}} - \ddot{\mathbf{q}}_\mathbf{d} + \lambda \dot{\mathbf{e}}. \tag{41}$$

Note that the equations of motion developed in section II-A take the form

$$M\ddot{\mathbf{q}} + \mathbf{a} = \mathbf{u}, \tag{42}$$

where

$$\mathbf{a} = \begin{bmatrix} a_1 & a_2 & a_3 & a_4 & a_5 \end{bmatrix}^T, \tag{43}$$

$$\mathbf{u} = \begin{bmatrix} F_x & F_y & F_l & 0 & 0 \end{bmatrix}^T. \tag{44}$$

Solving for $\ddot{\mathbf{q}}$ in (42) and substituting the result into (41), the derivative of the sliding surface is

$$\dot{\mathbf{s}} = -M^{-1}\mathbf{a} + M^{-1}\mathbf{u} - \ddot{\mathbf{q}}_\mathbf{d} + \lambda \dot{\mathbf{e}}. \tag{45}$$

Setting $\dot{\mathbf{s}} = 0$ and solving for the control action $\mathbf{u}$ results in

$$\mathbf{u} = M\ddot{\mathbf{q}}_\mathbf{d} - M\lambda \dot{\mathbf{e}} + \mathbf{a}. \tag{46}$$

A discontinuous term $k_i \text{sat}\left(\frac{s}{\Phi_i}\right)$ is added to the end of each control action $u_i$ to reduce chatter as the system approaches the sliding surface, where $k_i$ is a gain and $\Phi_i$ the width of the saturation region such that

$$\text{sat}\left(\frac{s}{\Phi_i}\right) = \begin{cases} \frac{s}{\Phi_i} & \text{if } |\frac{s}{\Phi_i}| \leq 1 \\ \text{sgn}(s) & \text{otherwise} \end{cases}. \tag{47}$$

For example, consider the first entry in $\mathbf{u}$, $u_1 = F_x$, and expanding (46) with the additional discontinuous term, one obtains

$$\begin{aligned} F_x =& M_{11}\left[\ddot{x}_d - \lambda_1(\dot{x} - \dot{x}_d)\right] + M_{13}\left[\ddot{l}_d - \lambda_3(\dot{l} - \dot{l}_d)\right] \\ &+ M_{14}\left[\ddot{\theta}_d - \lambda_4(\dot{\theta} - \dot{\theta}_d)\right] + a_1 \\ &- k_1 \text{sat}\left[\frac{\dot{x} - \dot{x}_d + \lambda_1(x - x_d)}{\Phi_1}\right]. \end{aligned} \tag{48}$$

*4) Fuzzy Logic Control:* An alternate approach to nonlinear control, an FLC does not require the derivation of the equations of motion of the system. Instead, FLC relies on predefined "rules" to control the system that are based on a physical intuition of how the system performs. The FLC built for the gantry crane system was developed based on the concepts presented in [11]. Fig. 5 shows the block diagram for the FLC implemented in LabVIEW. The inputs to the FLC are (25), the state error $e_q$, multiplied by a gain $G_{e,q}$, and the rate of change of the error $\dot{e}_q$, multiplied by a gain $G_{\dot{e},q}$. The output of the FLC is multiplied by gain $G_{u,q}$ to provide the control action.

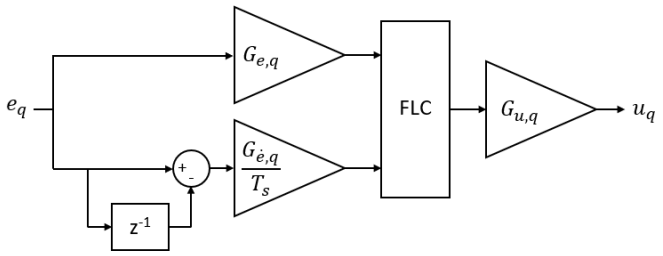


Fig. 5. Block diagram of the discrete-time LabVIEW FLC.

As with the PID controller, five FLCs are needed to control the system and dampen payload sway, one for each generalized coordinate, with the control efforts averaged using equations (26)-(28).

For each FLC, the universes of discourse for both $e$ and $\dot{e}$ were set to 5, and triangular membership functions were used. Fig. 6 presents the rule base for all of the FLCs.

| $u$ | | $\dot{e}$ | | | | |
|---|---|---|---|---|---|---|
| | | **-1** | **-0.5** | **0** | **0.5** | **1** |
| $e$ | **-1** | -1 | -1 | -1 | -0.5 | 0 |
| | **-0.5** | -1 | -1 | -0.5 | 0 | 0.5 |
| | **0** | -1 | -0.5 | 0 | 0.5 | 1 |
| | **0.5** | -0.5 | 0 | 0.5 | 1 | 1 |
| | **1** | 0 | 0.5 | 1 | 1 | 1 |

Fig. 6. Rule base for each FLC.

### *D. Input Shaping*

A method of open-loop control, input shaping aims to reduce vibration by shaping the input commands to avoid exciting the natural frequencies of the system. The input command sequence is convolved with a series of impulses with a delay based on the natural frequency of the system. In the present study input shapers are used to shape the trajectories sent to the feedback controllers, creating a control system that combines open and closed-loop control.

*1) Zero-Vibration Input Shaper:* As presented by Conker et al. [7], a ZV input shaper uses two impulses, with normalized amplitudes $A_1$ and $A_2$ applied at timesteps $t_1$ and $t_2$, and takes the form

$$ZV = \begin{bmatrix} A_1 & A_2 \\ t_1 & t_2 \end{bmatrix} = \begin{bmatrix} \frac{1}{1+K} & \frac{K}{1+K} \\ 0 & \frac{\pi}{\omega_d} \end{bmatrix} \tag{49}$$

where

$$K = e^{-\frac{\pi\zeta}{\sqrt{1-\zeta^2}}}, \tag{50}$$

$$\omega_d = \omega_n \sqrt{1-\zeta^2}. \tag{51}$$

In the present study no damping is considered, resulting in $K = 1$ and $\omega_d = \omega_n$. The natural frequency for a simple pendulum is $\omega_n = \sqrt{\frac{g}{l}}$. Using the initial pendulum length of $l_0 = 4$ metres, the ZV impulse sequence becomes

$$\begin{bmatrix} A_1 & A_2 \\ t_1 & t_2 \end{bmatrix} = \begin{bmatrix} 0.5 & 0.5 \\ 0 & 2 \end{bmatrix}. \tag{52}$$

*2) Zero-Vibration-Derivative Input Shaper:* A ZVD input shaper uses three impulses and takes the form

$$\begin{aligned} ZVD &= \begin{bmatrix} A_1 & A_2 & A_3 \\ t_1 & t_2 & t_3 \end{bmatrix} \\ &= \begin{bmatrix} \frac{1}{1+2K+K^2} & \frac{2K}{1+2K+K^2} & \frac{K^2}{1+2K+K^2} \\ 0 & \frac{\pi}{\omega_d} & \frac{2\pi}{\omega_d} \end{bmatrix} \end{aligned} \tag{53}$$

where $K$ and $w_d$ take the same values as for the ZV input shaper. The intention of adding an additional impulse is to make the input shaper more robust to errors identifying the natural frequency and damping ratio of the system [7].

*3) Zero-Vibration-Derivative-Derivative Input Shaper:* A ZVDD input shaper uses four impulses and takes the form

$$\begin{aligned} ZVDD &= \begin{bmatrix} A_1 & A_2 & A_3 & A_4 \\ t_1 & t_2 & t_3 & t_4 \end{bmatrix} \\ &= \begin{bmatrix} A_1 & A_2 & A_3 & A_4 \\ 0 & \frac{\pi}{\omega_d} & \frac{2\pi}{\omega_d} & \frac{3\pi}{\omega_d} \end{bmatrix} \end{aligned} \tag{54}$$

where

$$A_1 = \frac{1}{1+3K+3K^2+K^3}, \tag{55}$$

$$A_2 = \frac{3K}{1+3K+3K^2+K^3}, \tag{56}$$

$$A_3 = \frac{3K^2}{1+3K+3K^2+K^3}, \tag{57}$$

$$A_4 = \frac{K^3}{1+3K+3K^2+K^3}. \tag{58}$$

The addition of a fourth impulse is meant to further reduce the sensitivity of the shaper to errors in the natural frequency and damping ratio [7]. Note the additional impulses for the ZVD and ZVDD input shapers are further delayed from the impulses of the ZV. Using the parameters of the present system, (52) shows the second impulse of the ZV is applied at $t_2 = 2$ seconds. The third and fourth impulses of a ZVDD input shaper are applied at $t_3 = 4$ seconds and $t_4 = 6$ seconds, which will cause the system to have a noticeable delay for the operator.

## III. Results

### A. Tuning Trials - No Ship Motion

To tune each controller, trials were performed without ship motion using the predefined trajectories

$$\dot{x}_d = \dot{y}_d = \begin{cases} 0.3 \text{ m/s} & t < 12 \text{ s} \\ 0 \text{ m/s} & t \geq 12 \text{ s} \end{cases}, \tag{59}$$

$$\dot{l}_d = \begin{cases} 0 \text{ m/s} & t \leq 20 \text{ s} \\ 0.3 \text{ m/s} & 20 < t < 35 \text{ s} \\ 0 \text{ m/s} & t \geq 35 \text{ s} \end{cases}. \tag{60}$$

The gains for each controller were tuned heuristically, reducing the root-mean-square-error (RMSE) between the payload position and the desired trajectory, while keeping the sway angles below a maximum of $\theta_{max} = \phi_{max} = 2.5°$. As the MPC behaved differently than the other three controllers during tuning, the tuned gains and results for the PID, FLC and SMC are presented first, followed by a discussion on the MPC.

*1) PID, SMC and FLC:* The tuned gains for the PID, SMC and FLC are presented in Tables II, III, and IV, respectively. It was found through tuning that an integral gain was only required for the cable length PID controller, and did not provide an additional benefit for the other PID controllers.

TABLE II
PID Controller Gains

| | | |
|---|---|---|
| $K_{P,x} = 5E4$ | $K_{I,x} = 0$ | $K_{P,x} = 5E4$ |
| $K_{P,y} = 1.5E5$ | $K_{I,y} = 0$ | $K_{P,y} = 1.5E5$ |
| $K_{P,l} = 1E5$ | $K_{I,l} = 5E4$ | $K_{P,l} = 5E4$ |
| $K_{P,\theta} = 1.5E5$ | $K_{I,\theta} = 0$ | $K_{P,\theta} = 0$ |
| $K_{P,\phi} = 4.5E5$ | $K_{I,\phi} = 0$ | $K_{P,\phi} = 0$ |

TABLE III
SMC Controller Gains

| | | |
|---|---|---|
| $\lambda_1 = 2$ | $k_1 = 1E4$ | $\Phi_1 = 5$ |
| $\lambda_2 = 2$ | $k_2 = 2E4$ | $\Phi_2 = 5$ |
| $\lambda_3 = 5$ | $k_3 = 1E5$ | $\Phi_3 = 1$ |
| $\lambda_4 = 1$ | $k_4 = 0$ | $\Phi_4 = 1$ |
| $\lambda_5 = 1$ | $k_5 = 0$ | $\Phi_5 = 1$ |

TABLE IV
FLC Controller Gains

| | | |
|---|---|---|
| $G_{e,x} = 1$ | $G_{\dot{e},x} = 1$ | $G_{u,x} = 5E4$ |
| $G_{e,y} = 1$ | $G_{\dot{e},y} = 1$ | $G_{u,y} = 1.5E5$ |
| $G_{e,l} = 10$ | $G_{\dot{e},l} = 5$ | $G_{u,l} = 1E5$ |
| $G_{e,\theta} = 1$ | $G_{\dot{e},\theta} = 0$ | $G_{u,\theta} = 1.5E5$ |
| $G_{e,\phi} = 1$ | $G_{\dot{e},\phi} = 0$ | $G_{u,\phi} = 4.5E5$ |

As a basis to compare the performance of the controllers, the null control case was considered as a controller identical to the PID controller with all gains related to $\theta$ and $\phi$ set to zero. The null controller then provides trajectory control without direct anti-sway action.

Fig. 7 plots as a function of time the $x$ and $y$ positions of the payload and the cable length for the PID, SMC and FLC, as well as the null controller, using the predefined trajectories (59) and (60), without the addition of ship motion. The RMSE and maximum sway angles for each controller are presented in Table V.

As designed the PID, SMC and FLC all successfully track the trajectory and dampen out payload sway faster than the

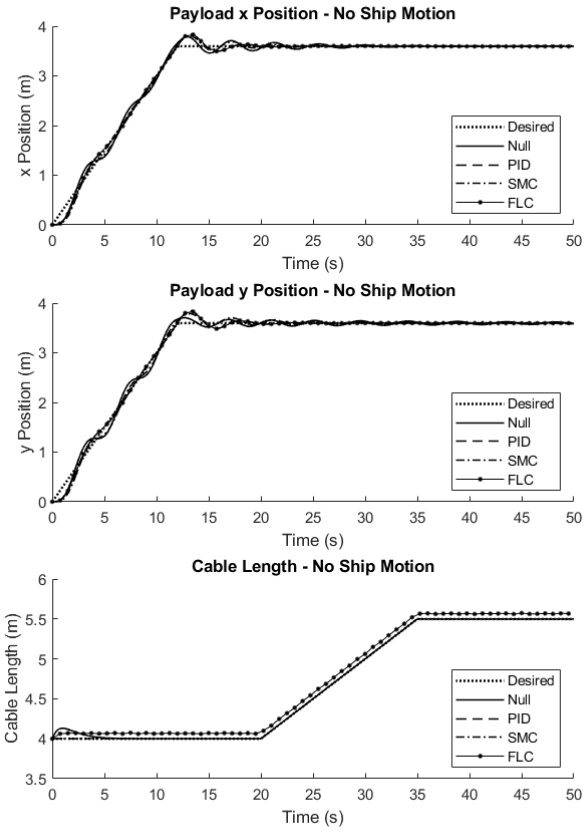


Fig. 7. Trajectory tracking performance of the PID, SMC and FLC, along with the null controller, without the addition of ship motion.

null control case, at the cost of a larger overshoot in $x$ and $y$. The PID and FLC provide almost identical performance for $x$ and $y$ position tracking; considering the inputs to the FLC are the trajectory error and rate of change of the error, the FLC is very similar in operation to a PD controller. However, the lack of an integral term in the current design of the FLC results in a steady-state error tracking the cable length setpoint. It was suspected that the non-linear SMC and FLC would show significant improvement over the PID, however all three provide a similar level of performance.

*2) MPC:* Unlike the PID, SMC and FLC, the MPC was unable to successfully track the desired trajectory due to the deadbands placed on the actuators. To be able to effectively tune the MPC, the deadbands had to be jumped. The prediction and control horizons were tuned to $N_p = 140$ and $N_c = 1$, and the output error weight matrix $Q$ for the MPC cost function tuned to

$$Q = \begin{bmatrix} 3E5 & 0 & 0 & 0 & 0 \\ 0 & 3E5 & 0 & 0 & 0 \\ 0 & 0 & 1E11 & 0 & 0 \\ 0 & 0 & 0 & 1E7 & 0 \\ 0 & 0 & 0 & 0 & 1E7 \end{bmatrix}. \quad (61)$$

Both the rate of change in control action weight matrix $R$ and the control action error weight matrix $N$ for the MPC cost function were set to $R = N = 0$, allowing the MPC to control the system with no regard for the magnitude or rate of change of the control action. Additionally, no constraints were added to the MPC. Table V provides the RMSE and maximum sway angles for the tuned MPC with the deadbands jumped.

Fig. 8 shows the performance of the MPC controller with and without jumping the deadbands. Without jumping the deadbands, the state-space model provides inaccurate predictions for the current state of the system, as any forces within the deadbands provide a change in state for the state-space model, but not for the actual system. Note that for the PID, SMC and FLC the deadbands result in limit cycles as the system approaches steady state. As the amplitudes of the limit cycles are on the order of $10^{-3}$ metres and smaller, there is negligible effect on performance.

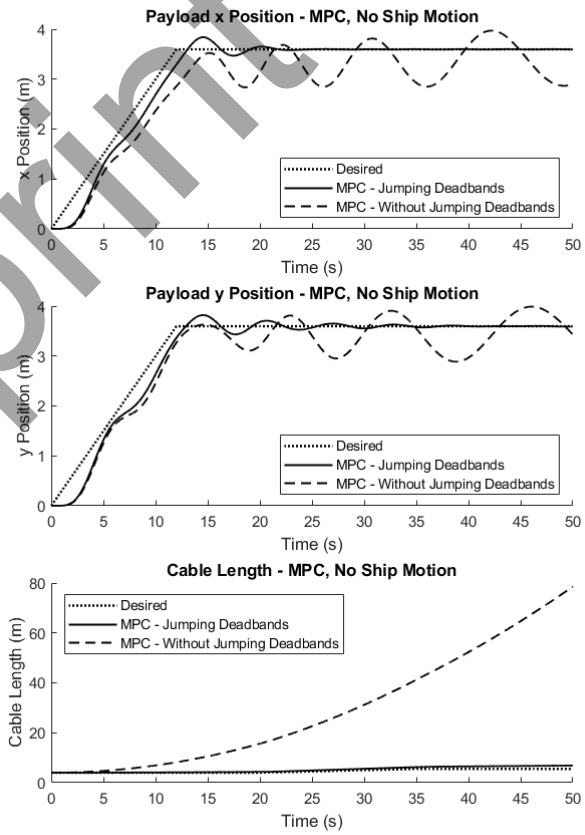


Fig. 8. Trajectory tracking performance of the MPC controller with and without jumping the deadbands of all three actuators.

Even with jumping the deadbands, Fig. 8 shows drift in cable length for the MPC due to the linearized equations of motion, albeit significantly less drift than without jumping the deadbands. As the payload swings and the system moves away from the linearized operating point, the mismatch between the control action predicted by the linearized MPC and the force

actually required by the non-linear system result in a non-zero acceleration, causing drift. Woodacre et al. [12] encounter a similar MPC drift when implementing anti-heave control with an MPC on a hydraulic winch system, and correct the issue with a PI controller operating in parallel with the MPC.

TABLE V
RMSE AND MAXIMUM SWAY ANGLES - NO SHIP MOTION

| Trajectory | RMSE (m) | | | | |
|---|---|---|---|---|---|
| | ***Null*** | ***PID*** | ***MPC*** | ***SMC*** | ***FLC*** |
| $x$ | 0.071 | 0.062 | 0.179 | 0.063 | 0.062 |
| $y$ | 0.075 | 0.061 | 0.186 | 0.071 | 0.062 |
| $l$ | 0.025 | 0.025 | 0.676 | 2.2E-4 | 0.067 |
| **Angle** | **Maximum Sway Angles (°)** | | | | |
| $\theta_{max}$ | 2.71 | 2.26 | 1.55 | 2.27 | 2.25 |
| $\phi_{max}$ | 2.87 | 2.40 | 1.59 | 2.39 | 2.38 |

### *B. Input Shaping - No Ship Motion*

All four controllers, along with the null controller, were tested with the addition of a ZV, ZVD and ZVDD input shaper to observe any improvements in performance. The deadbands were jumped for the MPC to allow the controller to track the desired $x$ and $y$ trajectories. Figures 9, 10, 11 and 12 present the performance of the PID, MPC, SMC and FLC controllers, respectively, with each input shaper. Table VI presents the maximum sway angles experienced by the payload during each trial; as the input shapers cause a delay in response, all of the controllers showed a significantly increased RMSE with input shaping. Since the primary objective of the control system is sway reduction, RMSE will not be used to evaluate the performance of the input shapers. Note also that input shaping was only applied to the $x$ and $y$ trajectories; as varying the cable length does not excite the natural frequency of the pendulum, the addition of input shaping for the $l$ trajectory was not found to be beneficial.

TABLE VI
MAXIMUM SWAY ANGLES - NO SHIP MOTION

| Input Shaping | $\theta_{max}$ (°) | | | | |
|---|---|---|---|---|---|
| | ***Null*** | ***PID*** | ***MPC*** | ***SMC*** | ***FLC*** |
| None | 2.71 | 2.26 | 1.47 | 2.27 | 2.25 |
| ZV | 1.41 | 1.16 | 0.78 | 1.28 | 1.15 |
| ZVD | 0.83 | 0.91 | 0.59 | 0.90 | 0.91 |
| ZVDD | 0.76 | 0.74 | 0.47 | 0.72 | 0.74 |
| | $\phi_{max}$ (°) | | | | |
| None | 2.87 | 2.40 | 1.52 | 2.39 | 2.38 |
| ZV | 1.51 | 1.18 | 0.83 | 1.24 | 1.17 |
| ZVD | 0.75 | 0.88 | 0.67 | 0.74 | 0.88 |
| ZVDD | 0.75 | 0.75 | 0.56 | 0.70 | 0.74 |

The addition of an input shaper for each controller significantly reduced the maximum sway angles, with the ZVDD showing the greatest reduction in payload sway in every case. However, input shaping also causes a significant delay in trajectory response as more impulses are used with each input shaper. Due to the low natural frequency of the system and the length of the delays, human operators will have difficulty controlling the system. Therefore, given the results of the

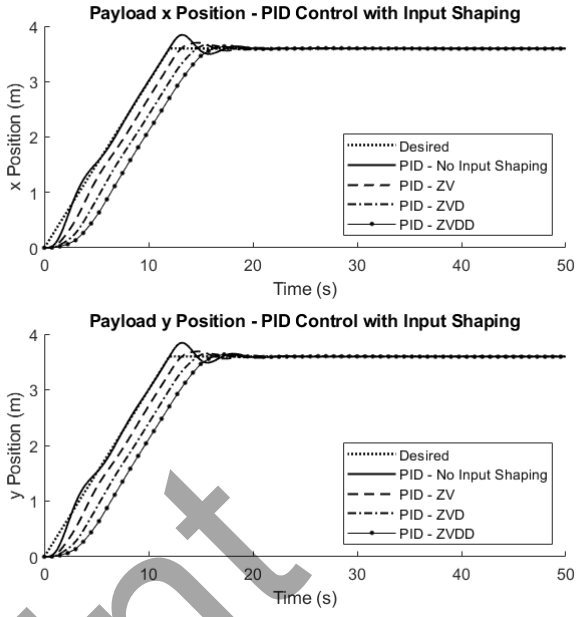


Fig. 9. Trajectory tracking performance of the PID controller with a ZV, ZVD and ZVDD input shaper, without disturbances from ship motion.

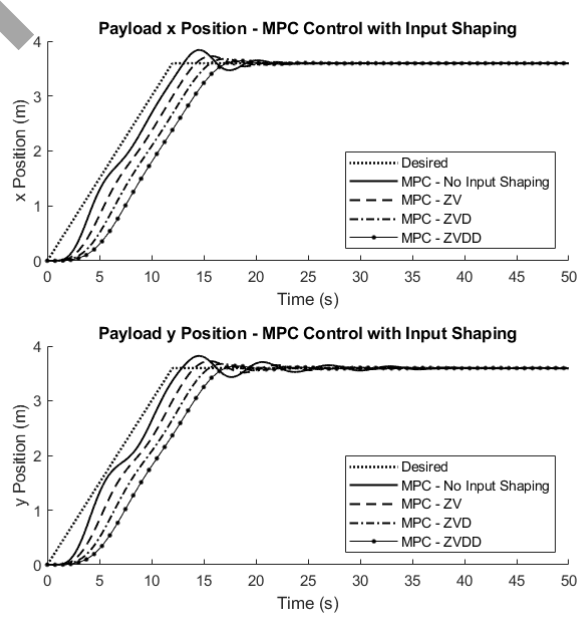


Fig. 10. Trajectory tracking performance of the MPC with a ZV, ZVD and ZVDD input shaper, without disturbances from ship motion.

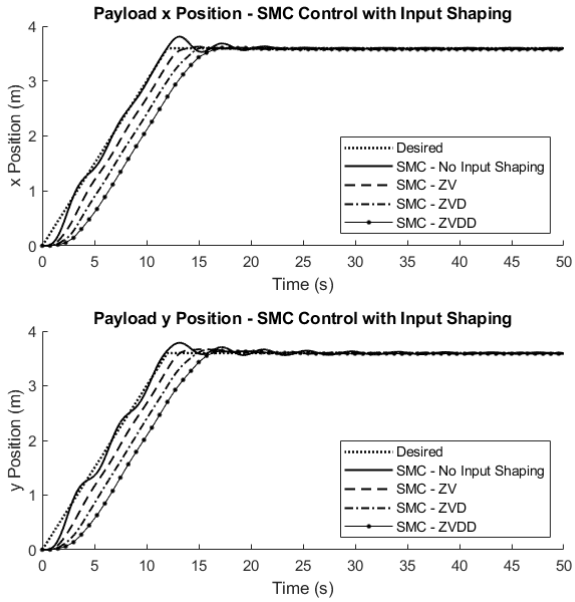


Fig. 11. Trajectory tracking performance of the SMC with a ZV, ZVD and ZVDD input shaper, without disturbances from ship motion.

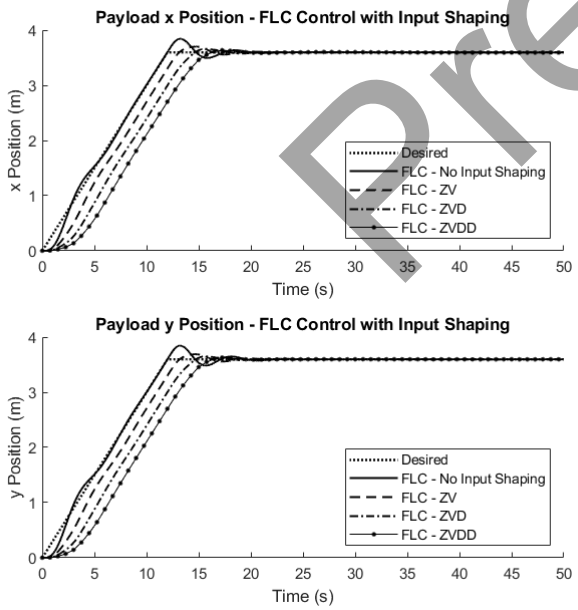


Fig. 12. Trajectory tracking performance of the FLC with a ZV, ZVD and ZVDD input shaper, without disturbances from ship motion.

present study it is recommended that input shaping should only be deployed for automated or autonomous crane systems.

### C. Ship Motion

The four controllers were then tested with 6-axis ship motion actuating the base of the crane. The ship motion data was generated with ShipMo3D [13] for sea state 6. The sea way was modelled with regular waves of the Bretschneider spectrum using a significant wave height of 5 m and a period of 2.4 seconds. The ship was the generic frigate included in ShipMo3D [13], sailing at a speed of 6.000 kt with a heading of 15.0° into the sea. A summary of the ship motion is presented in Table VII. The frequency of the roll, pitch and yaw ship motion was 0.093 Hz.

TABLE VII
SHIP MOTION PARAMETERS

| | ***Surge* (m)** | ***Sway* (m)** | ***Heave* (m)** | ***Roll* (°)** | ***Pitch* (°)** | ***Yaw* (°)** |
|---|---|---|---|---|---|---|
| Maximum | 0.993 | 0.279 | 1.280 | 1.920 | 2.270 | 0.345 |
| Minimum | -0.993 | -0.279 | -1.280 | -1.920 | -2.270 | -0.345 |
| RMS | 0.701 | 0.197 | 0.908 | 1.360 | 1.600 | 0.244 |

Fig. 13 presents the payload position and cable length for the ship motion trials with the PID, SMC and FLC controllers without input shaping. Table VIII presents the maximum sway angles experienced by the payload for the PID, SMC and FLC for each trial with the addition of a ZV, ZVD and ZVDD input shaper

TABLE VIII
MAXIMUM SWAY ANGLES - WITH SHIP MOTION

| **Input Shaping** | $\theta_{max}$ (°) | | | |
|---|---|---|---|---|
| | ***Null*** | ***PID*** | ***SMC*** | ***FLC*** |
| None | 5.14 | 3.73 | 3.97 | 3.78 |
| ZV | 4.40 | 3.86 | 3.90 | 3.85 |
| ZVD | 4.27 | 3.39 | 3.50 | 3.40 |
| ZVDD | 4.14 | 3.26 | 3.10 | 3.27 |
| | $\phi_{max}$ (°) | | | |
| None | 6.78 | 5.24 | 5.63 | 5.24 |
| ZV | 3.92 | 4.04 | 3.68 | 4.04 |
| ZVD | 3.38 | 3.51 | 3.29 | 3.51 |
| ZVDD | 3.39 | 3.36 | 3.31 | 3.37 |

As designed none of the controllers are able to track the desired trajectory in the presence of ship motion, and the addition of anti-sway control appears to cause larger trajectory errors compared to the null control case. The addition of input shaping does appear to reduce payload sway in some cases, however alone is insufficient. The results of the MPC are not shown, as when tested the system showed substantial drift and was unable to maintain the payload near the desired trajectory.

It is possible the use of a signal prediction algorithm, such as developed by McPhee and Irani [14] could provide disturbance information to the MPC. With a PI controller in parallel to correct drift, it is possible the MPC could control the system in the presence of ship motion.

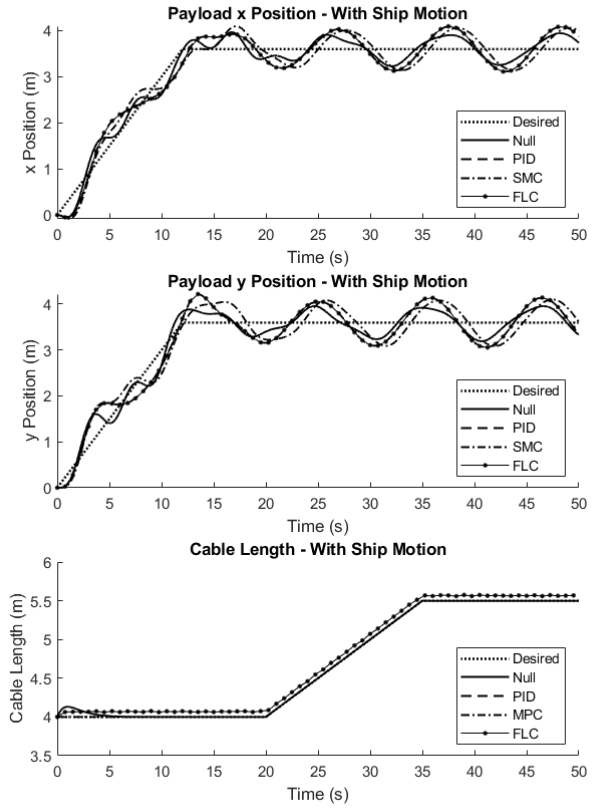


Fig. 13. Trajectory tracking performance of the PID, SMC and FLC controller with disturbances from ship motion.

## IV. Conclusion

A simulation tool that allows the examination of the control to a five degree-of-freedom shipboard gantry crane was successfully developed. Additionally, the simulator allows the operator to provide input trajectories and receive visual feedback of the system through a 3D render of the crane.

A proportional-integral-derivative controller, model predictive controller, sliding mode controller and fuzzy logic controller were all developed for the crane and operate in real-time on a NI myRIO. The PID, SMC and FLC were all successful at tracking a desired trajectory and dampening payload sway without disturbances from ship motion. The MPC was unable to control the system without jumping the actuator deadbands, and a PI controller would be needed to correct drift. Additionally, as designed none of the controllers were successful at tracking the desired trajectory in the presence of ship motion.

Given the results of the present study, it appears that PID controllers still have use in industrial crane applications. The results indicate that the additional effort required to develop an SMC or FLC provides negligible benefit over a PID, despite the system being non-linear.

The addition of an input shaper showed a significant reduction in payload sway for all of the controllers, but also showed a significant delay in system response. Given the results of the present study, input shaping should only be deployed on automated or autonomous crane systems.

With the simulation tool developed, future work will focus on improving the controllers to reduce the payload sway in the presence of ship motion. A signal prediction algorithm for an MPC-PI controller could also be explored to improve the system. Additionally, operator-in-the-loop testing will be performed and the controllers deployed to a laboratory scale robotic crane to validate the simulation results.

## Acknowledgment

The authors would like to thank the Natural Sciences and Engineering Research Council of Canada (NSERC) for their financial support, and Dynamics Systems Analysis Ltd (DSA LTD) for the in-kind donation of ShipMo3D. The authors would also like to acknowledge the contribution of R. McKenzie for their work on TCP communication between Simulink and LabVIEW and their assistance in implementing MPC in LabVIEW.

## References

[1] L. Ramli *et al.*, "Control strategies for crane systems: A comprehensive review," *Mechanical Systems and Signal Processing*, vol. 95, pp. 1–23, 2017.

[2] Y. Qian, Y. Fang, and B. Lu, "Adaptive repetitive learning control for an offshore boom crane," *Automatica*, vol. 82, pp. 21–28, 2017.

[3] Q. Ngo and K. Hong, "Adaptive sliding mode control of container cranes," *IET Control Theory and Applications*, vol. 6(5), pp. 662–668, 2012.

[4] L. Tuan *et al.*, "Adaptive neural network sliding mode control of shipboard container cranes considering actuator backlash," *Mechanical Systems and Signal Processing*, vol. 112, pp. 233–250, 2018.

[5] Y. Qian, Y. Fang, and B. Lu, "Adaptive robust tracking control for an offshore ship-mounted crane subject to unmatched sea wave disturbances," *Mechanical Systems and Signal Processing*, vol. 114, pp. 556–570, 2019.

[6] T. Yang *et al.*, "Neural network-based adaptive antiswing control of an underactuated ship-mounted crane with roll motions and input dead zones," *IEEE Transactions on Neural Networks and Learning Systems*, vol. Ahead of Print, 2019.

[7] C. Conker, H. Yavuz, and H. Bilgic, "A review of command shaping techniques for elimination of residual vibrations in flexible-joint manipulators," *Journal of Vibroengineering*, vol. 18(5), pp. 2947–2958, 2016.

[8] Zodiac-Nautic.com, "Open 6.5," [Online]. Available: https://www.zodiac-nautic.com/en/shop/produits/boats/open-en/open-6-5, [Accessed: 15-Mar-2019].

[9] National Instruments, *LabVIEW Control Design User Manual*. National Instruments Corporation, 2009.

[10] J. Slotine and W. Li, *Applied Nonlinear Control*. Prentice-Hall, Inc, 1991.

[11] K. Passino and S. Yurkovich, *Fuzzy Control*. Addison Wesley Longman, Inc, 1998.

[12] J. Woodacre, R. Bauer, and R. Irani, "Hydraulic valve-based active-heave compensation using a model-predictive controller with non-linear valve compensations," *Ocean Engineering*, vol. 152, pp. 47–56, 2018.

[13] DSA-Ltd, "Shipmo3d," [Online]. Available: https://dsa-ltd.ca/shipmo3d/overview/, [Accessed: 19-Aug-2019].

[14] J. McPhee and R. Irani, "On-line determination of a go-nogo state using a continuous estimation of the system response," in *Proceedings of The Canadian Society for Mechanical Engineering International Congress 2018 (CSME 2018)*, 2018.